Unconventional Ballooning Structures for Toroidal Micro-instabilities

Hua-sheng XIE (谢华生, huashengxie@gmail.com) and Yong XIAO

Institute for Fusion Theory and Simulation, Department of Physics,
Zhejiang University, Hangzhou 310027, P.R.China

International Sherwood Fusion Theory Conference,
Mar. 16-18, 2015, New York, USA

Ackn.: L. Chen, H. T. Chen, Z. Lin / GTC team, T. Xie, Z. X. Lu, D. Dickinson, · · ·

Institute for Fusion Theory and Simulation, Zhejiang University

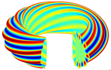

Background

1. **Drift waves / micro-instabilities**, universally in magnetized plasmas, believed to be cause of anomalous transport.

2. **Conventional** ballooning structures peak at outboard side of cross section, with poloidal angle position $\theta_p \simeq 0$. Unconventional, $|\theta_p| \simeq$ or $< \pi/2$ have shown exist by several authors [Xie12, Dickinson14, Singh14, Fulton14].

3. We will **show even more general unconventional results**. **Theory** to explain them is also **provided.**

4. To find **differences of micro-instabilities between H-mode and L-mode**.

TEMs in GTC

Fig.1: Conventional (a) & unconventional (b-i) ballooning structures of TEMs in GTC simulations. (a) weak gradient L-mode (Cyclone case) parameter, (b)-(i) strong gradient H-mode parameters. Collision included in (e) & (g). Flow excluded in all cases.

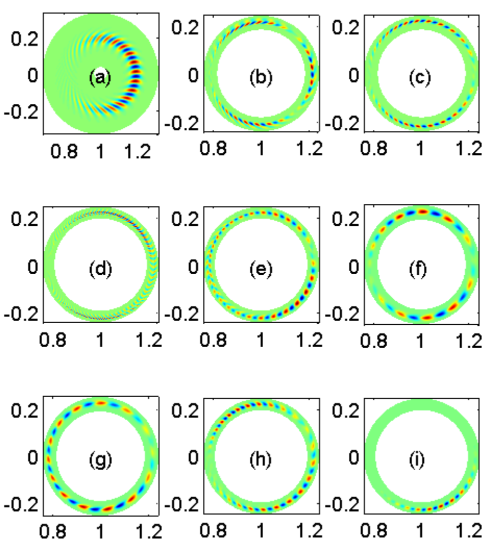

Figure 1: TEMs in GTC.

TEMs in GTC

Parameters: HL-2A H-mode. Single-n ($n = 5 - 30$).

$B_0 = 1.35T$, $a = 40cm$, $R_0 = 165cm$, $q = 2.5 - 3.0$, $s = 0.3 - 1.0$,
$R_0/L_T = 80 - 160$ and $T_e(r) = T_i(r)$, $n_e(r) = n_i(r)$, $\eta = L_n/L_T \simeq 1.0$.

Most unexpected unconventional new features:

- a. mode can have **anti-ballooning** structure ($|\theta_p| > \pi/2$, e.g., Fig.1g);
- b. mode can have **multi-peak** positions (e.g., Fig.1b).

TEMs Fourier $\delta\phi_m(r)$

$$\delta\phi(r,\theta,\zeta) = e^{in\zeta}\sum_m \delta\phi_m(r)e^{-im\theta}$$

Fig.2: Corresponding polodial cross section mode structures of (a)-(d) taken from Fig.1 (a), (b), (g) and (i), respectively.

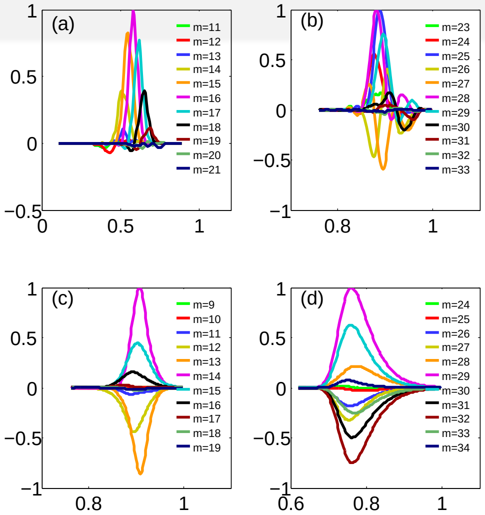

Figure 2: $\Re[\delta\phi_m(r)]$ for conventional and unconventional mode structures.

TEMs Fourier $\delta\phi_m(r)$

- Conventional $\delta\phi_m \simeq \delta\phi_{m+1}$; unconventional relation between $\delta\phi_m$ and $\delta\phi_{m+1}$ no longer apparent.

- Fig.2b, several $\delta\phi_m$ are **not Gaussian shapes as in Fig.2a**; two strongest Fourier modes in **Fig.2c&d have anti-phase, i.e.,** $\delta\phi_{m_a} \simeq -\delta\phi_{m_b}$. Difference of Fig.2c&d is $m_b = m_a + 1$ in Fig.2c but $m_b = m_a + 3$ in Fig.2d.

ITG in GTC

Reducing density gradient, ITG can unstable. **Adiabatic electron** in simulations, to exclude TEM.

Fig.3: (a & b) Anti-ballooning structure. (c & d) Two modes co-exist (or, one mode with two radius peaks) at different radius positions. One $\theta_p \simeq \pi/2$, another $\theta_p \simeq -\pi/2$.

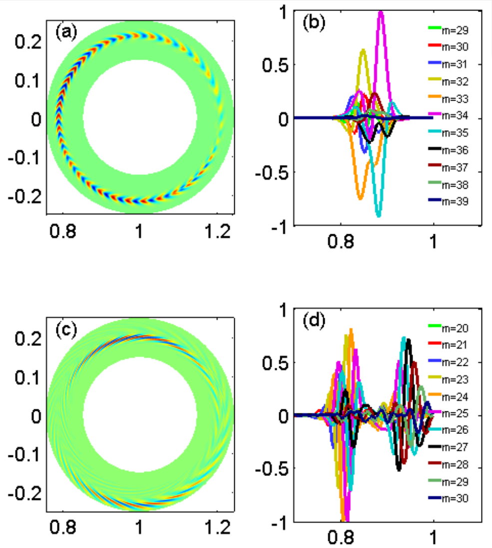

Figure 3: Unconventional ITG in GTC.

ITG in GTC

- **Unconventional mode structures still exist** and can be more rich. Thus, these unconventional properties **can be common for drift waves, not limited to TEM**.

- Anti-ballooning ITG shown in Fig.3a&b. Actually, mode structures with global profiles and multi modes co-exist in initial value simulations will be more complicated. Two modes with similar growth rates can be excited in different radius (Fig.3c&d). Multi modes coexist with close peaking positions in initial simulation can also lead $\theta_p = \theta_p(t)$, i.e., 'rotate' with time.

- These unconventional linear behaviors in GK simulations **can be understood from the below eigen analysis**.

Starting equation

Qualitative model theory by solve below model eigenvalue problem

$$\left[\rho_i^2\frac{\partial^2}{\partial x^2}-\frac{\sigma^2}{\omega^2}\left(\frac{\partial}{\partial\theta}+ik_\theta sx\right)^2-\frac{2\epsilon_n}{\omega}\left(\cos\theta+\frac{i\sin\theta}{k_\theta}\frac{\partial}{\partial x}\right)\right.$$
$$\left.-\frac{\omega-1}{\omega+\eta_s}-k_\theta^2\rho_i^2\right]\delta\phi(x,\theta)=0, \quad (1)$$

$\sigma=\epsilon_n/(qk_\theta\rho_i)$, $\eta_s=1+\eta_i$, $x=r-r_s$, the poloidal wave number $k_\theta=nq/r$. Eq.(1) can be derived from gyrokinetic theory with adiabatic electron assumption, thus can be used to study ITG.

We solve...

- **1D**: Corresponding 1D equation in ballooning space

$$\Big\{\frac{\sigma^2}{\omega^2}\frac{d^2}{d\vartheta^2}+k_\theta^2\rho_i^2[1+s^2(\vartheta-\vartheta_k)^2]+\frac{2\epsilon_n}{\omega}[\cos\vartheta$$
$$+s(\vartheta-\vartheta_k)\sin\vartheta]+\frac{\omega-1}{\omega+\eta_s}\Big\}\delta\hat{\phi}(\vartheta,\vartheta_k)=0, \qquad (2)$$

ϑ_k ballooning-angle parameter.

- **2D**: Using Fourier basis $\delta\phi(x,\theta)=\sum_m u_m e^{-im\theta}$, Eq.(1) can rewritten to

$$k_\theta^2\rho_i^2 s^2\frac{\partial^2 u_m}{\partial z^2}+\frac{\sigma^2}{\omega^2}(z-m)^2 u_m-\frac{\epsilon_n}{\omega}\Big[\Big(1-s\frac{\partial}{\partial z}\Big)u_{m-1}$$
$$+\Big(1+s\frac{\partial}{\partial z}\Big)u_{m-1}\Big]-\Big(\frac{\omega-1}{\omega+\eta_s}+k_\theta^2\rho_i^2\Big)u_m=0, \qquad (3)$$

$z=k_\theta sx$. To solve eigenvalue problem Eq.(3), only several m modes need kept.

Analytical investigations

With suitable approximations, Eqs.(2) & (3) reduced to Weber equation $u'' + (bx^2 + a)u = 0$, solutions

- eigenvalues $a(\omega) = i(2l + 1)\sqrt{b(\omega)}$
- eigenfunctions $u(x) = H_l(i\sqrt{b}x)e^{-ibx^2/2}$,

H_l is l-th Hermite polynomial and $l = 0, 1, 2, ...,$ series eigenstates.

Numerical method

- Eqs.(2) & (3) to $\omega^3\mathbf{M}_3\mathbf{X}+\omega^2\mathbf{M}_2\mathbf{X}+\omega\mathbf{M}_1\mathbf{X}+\mathbf{M}_0\mathbf{X}=0$. Finite difference discrete yields sparse matrices $\mathbf{M}_i$ $(i=0,1,2,3)$.

- Using **companion matrix**, to $\mathbf{AY}=\omega\mathbf{BY}$, $\mathbf{Y}=[\mathbf{X}_1,\mathbf{X}_2,\mathbf{X}_3]\equiv[\mathbf{X},\omega\mathbf{X},\omega^2\mathbf{X}]$, $\mathbf{A}=[\mathbf{O},\mathbf{I},\mathbf{O};\mathbf{O},\mathbf{O},\mathbf{I};-\mathbf{M}_0,-\mathbf{M}_1,-\mathbf{M}_2]$, $\mathbf{B}=[\mathbf{I},\mathbf{O},\mathbf{O};\mathbf{O},\mathbf{I},\mathbf{O};\mathbf{O},\mathbf{O},\mathbf{M}_3]$.

- **All solutions of the system can obtained** by standard matrix solver. Advantage: **can show completely solutions of the system and help to understand transition and distribution of them**.

- **Solutions in [Xie12,Dickinson14]** using iterative solver are actually only one of solutions and **usually not most unstable or most important**, due to initial guess.

Eigen 1D solutions

1D Eq.(2), **unconventional structures either most unstable solution $l \neq 0$ or $\vartheta_k \neq 0$**. Both can happen at strong gradient. Most unstable solution $\vartheta_k \neq 0$ has discussed by others (c.f., [Singh14]).

Fig.4: **Weak gradient ($\epsilon_n = 0.5$), most unstable solution ground state (a&b)**, conventional structure. **Strong gradient ($\epsilon_n = 0.2$), most unstable solution not ground state (c&d)**, unconventional.

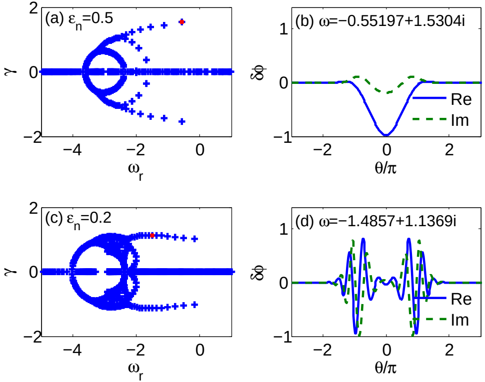

Figure 4: Eq.(2), series solutions exist. ($s = 0.8$, $k_\theta \rho_i = 0.4$, $q = 1.0$, $\eta_s = 3.0$ and $\vartheta_k = 0$)

Important Result!!!

Eigen 2D solutions

Almost all mode structures in Figs.1 & 3 also found in 2D solutions Eq.(3). Two examples in Fig.5. Thus, series conventional and unconventional solutions found in both 2D eigen solver and GTC initial simulations.

Condition $\epsilon_n < \epsilon_c$, critical gradient parameter ϵ_c depends on other parameters. GTC simulations HL-2A parameters, **typical critical gradient value** $R_0/L_T = 40 - 120$.

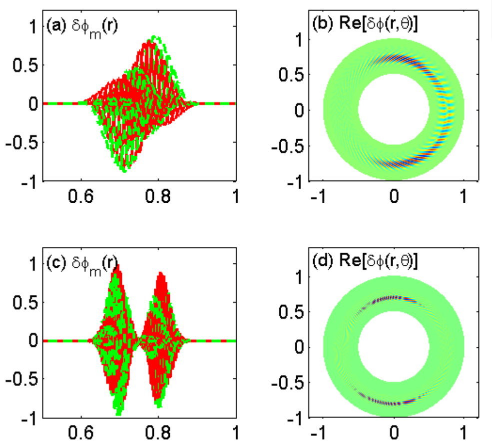

Figure 5: Typical unconventional mode structures from 2D eigen solution for Eq.(3). (b) similar Fig.1(c&d), and (c&d) similar Fig.3(c&d).

Physical picture

- With strong gradient the most unstable solution can shift from ground state to other non-ground states, which is **analogous to the quantum jump between energy levels**.
- Physically, the **'quanta' jump behaviors can be understood from the effective potential[Chen80]**. Jump happens from one potential well to another, which leads to different energy levels.

Discussions

- Strong gradient (H-mode) $l \neq 0$ v.s. weak gradient (L-mode) $l = 0$, indicate different transport behavior between H-mode and L-mode.

- Conventional, neighboring Fourier $u_m \simeq u_{m+1}$, effective correlation length estimated as width of radial envelope of the modes, say, ΔA. Whereas, unconventional, especially anti-ballooning, $u_m \simeq -u_{m+1}$, i.e., a 180° phase shift for neighboring Fourier, which can change correlation length to distance of neighboring mode-rational surfaces Δr_s.

- Considering that $\Delta r_s \ll \Delta A$, we can expect that **H-mode can have better confinement**.

- However, to fully understand, systematic study of nonlinear behavior of transport required (**See backup slides, HL-2A H-mode TEM nonlinear indeed differs from L-mode!!**).

Summary

1. **Broad class of unconventional ballooning modes found** for ES drift waves (TEM and ITG) by gyrokinetic simulations, shown to be **common in strong gradient** regime.
2. These unconventional mode structures are shown to correspond to **non-ground-state solutions** of the eigen mode equation.
3. These results may have important implications for turbulent transport in tokamaks, i.e., turbulent transport mechanism in **H-mode can be rather different from that in L-mode**.

HL-2A linear jump from L to H

Fig.6: Linear frequency and growth rate vs. different temperature & density gradient. Frequency has a **jump from $\omega > 10\omega_s$ to $\omega < 3\omega_s$** (a) if normalized half width Δ/a of the pedestal larger than 0.08 with nonuniform gradient, or (b) if gradient parameter $RL_T^{-1} < 80$ for flatten gradient.

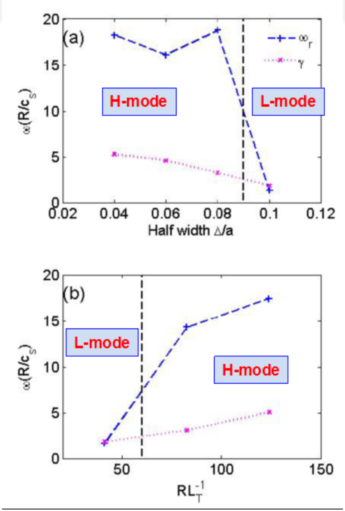

Figure 6: HL-2A linear jump from L to H

Nonlinear TEM (preliminary)

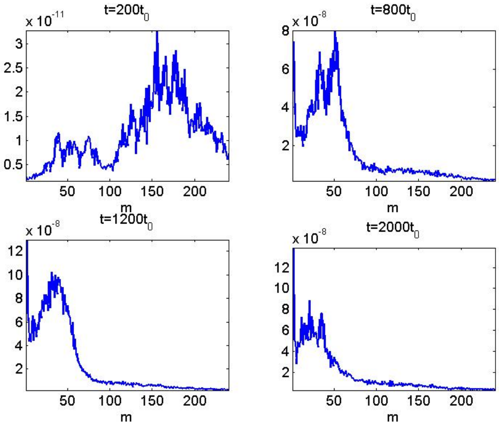

Figure 7: Poloidal power spectra of electrostatic potential for different time steps. **NL inverse cascading makes peaking m downshift** from large number to $m = 12 - 38$, which close to experimental value $m = 14 - 33$.

Nonlinear TEM (preliminary)

Fig.8: n=05 to 25 single-n simulation; zf=0 all n kept but zonal flow and density removed; zf=2 all n include zonal mode kept.

$t = 800t_0$, dominate is $n \simeq 20 - 25$ gives $m \simeq nq \simeq 65$; $t = 1200t_0$, $n \simeq 15$ gives $m \simeq nq \simeq 40$; $t = 2000t_0$, $n \simeq 10$ gives $m \simeq nq \simeq 26$.

Close to multi-n results (Fig.7), **reveal multi-mode-coupling not an important factor for m downshift as in L-mode** [e.g., Wang07, Lang08].

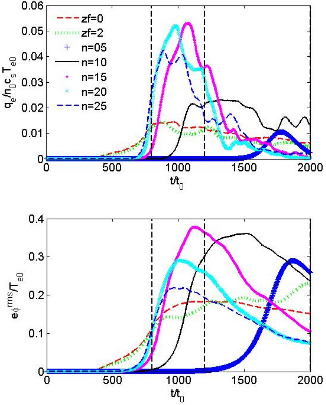

Figure 8: Time history of root-mean-square of $\delta\phi(t)$ and electron energy flux for single-n mode and multi-n modes NL simulations.